Three-Dimensional Atomic Force Microscopy: Interaction Force Vector by Direct Observation of Tip Trajectory
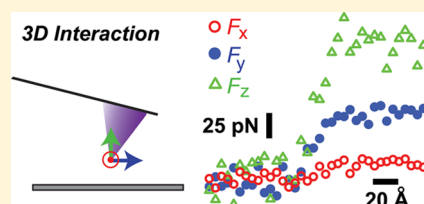
Krishna P. Sigdel,[†] Justin S. Grayer,[†] and Gavin M. King*[,†,‡]

[†]Department of Physics and Astronomy and [‡]Joint with the Department of Biochemistry, University of Missouri-Columbia, Columbia, Missouri 65211

Ⓢ Supporting Information

ABSTRACT: The prospect of a robust three-dimensional atomic force microscope (AFM) holds significant promise in nanoscience. Yet, in conventional AFM, the tip–sample interaction force vector is not directly accessible. We scatter a focused laser directly off an AFM tip apex to rapidly and precisely measure the tapping tip trajectory in three-dimensional space. This data also yields three-dimensional cantilever spring constants, effective masses, and hence, the tip–sample interaction force components via Newton's second law. Significant lateral forces representing 49 and 13% of the normal force ($F_z = 152 \pm 17$ pN) were observed in common tapping mode conditions as a silicon tip intermittently contacted a glass substrate in aqueous solution; as a consequence, the direction of the force vector tilted considerably more than expected. When addressing the surface of a lipid bilayer, the behavior of the force components differed significantly from that observed on glass. This is attributed to the lateral mobility of the lipid membrane coupled with its elastic properties. Direct access to interaction components F_x, F_y, and F_z provides a more complete view of tip dynamics that underlie force microscope operation and can form the foundation of a three-dimensional AFM in a plurality of conditions.

KEYWORDS: AFM, 3D, pointing noise, normal, lateral, back scattered

The atomic force microscope (AFM) is a ubiquitous tool across nanoscience.[1,2] The technique owes its popularity to its combination of high-resolution coupled with high versatility; it can operate equally well in vacuum and in liquid environments, as well as on conducting and insulating specimens. The heart of an AFM consists of a sharp tip affixed to the end of a compliant cantilever. In conventional AFM, the local three-dimensional (3D) position of the tip is not observable; instead, the vertical deflection (bending) ΔZ of the cantilever away from its equilibrium position is measured.[3,4] This observable yields force.

In most imaging and spectroscopy applications, force measurements are made in the z direction, that is, normal to the sample surface. However, torsional deflection (twisting) of the cantilever can also be monitored, as in frictional force microscopy.[5] In both cases, tip motion, which occurs in three dimensions, is convolved into angular displacements of the cantilever. It is challenging to infer 3D tip trajectories from this reduced coordinate system, even if the geometry of the tip and its orientation relative to the sample are known. This is because tip and cantilever dynamics are not always in lock-step with each other as transient excitations can propagate along the flexible cantilever, especially during fast scanning.[6,7] Furthermore, frictional coupling between the tip and sample causes complex dynamics, such as cantilever bowing and tip slipping that are convolved with the ΔZ signal.[8−10]

Despite limitations, researchers have utilized the conventional AFM observables to achieve numerous powerful insights. Three-dimensional AFM[11−17] represents an exciting capability which, for example, has recently been utilized to measure the force required to move a single atom on a surface in vacuum[13] and map surface hydration layers in fluid.[14] In a powerful implementation, a large amount of frequency shift data are collected at various lateral positions and then analyzed, leading to the assignment of 3D interaction force vectors with atomic precision.[13,17] This process can take hours to complete, which limits the types of samples that can be studied as well as the experimental conditions. An alternative approach has reduced the acquisition time scale significantly;[14,18] however, the method still relies on an inherently one-dimensional observable.

In this Letter, we report 3D force measurements based on a 3D local observable, rather than on cantilever deflection alone. By directly observing the three-dimensional tapping mode tip trajectory, we rapidly (10 ms) and precisely ($\sigma \leq 17$ pN) measure the interaction force components at arbitrary points in space in a room-temperature fluid. The approach yields the 3D force components without the need for lateral scanning. Thus, it places minimal restrictions on experiments.

Our measurements build upon ultrastable AFM,[19] a recently developed technique that was inspired by surface-coupled optical trapping microscopy methods. Ultrastable AFM employs a focused laser that backscatters off the tip itself to rapidly yield tip position with high spatial precision in 3D. In previous work, this tip-position data was used to stabilize the tip

with respect to a surface in contact mode and in air.[19] Here, we extend that work to the commonly applied intermittent contact (tapping)[20] mode in fluid and use the positional data to achieve different ends. In particular, measurements of 3D tip trajectories allowed determination of spring constants, resonance frequencies, and effective masses for the three degrees of freedom of the tip. Measurements of tip acceleration in 3D allowed determination of the 3D interaction force by applying Newton's second law of motion.

A schematic diagram of the apparatus is shown in Figure 1. As in conventional AFM,[3] a laser beam (λ_1 = 785 nm) was
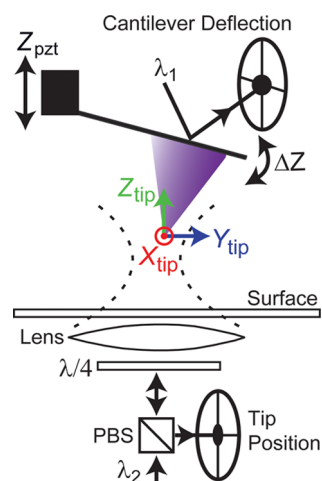

Figure 1. Schematic of the apparatus. The combination of 3D tip position measurement (X_{tip}, Y_{tip}, Z_{tip}) with conventional force detection is shown. An optical lever arm laser (λ_1) is reflected off the back of the cantilever to yield ΔZ. A separate laser (λ_2) is focused onto the tip apex using an objective lens positioned under the sample. Backscattered light from the tip is collected by the same lens and detected using a quadrant photo detector, yielding the three-dimensional tip position.

reflected off the backside of the cantilever and incident upon a quadrant photodiode (QPD) to yield ΔZ, the cantilever deflection away from equilibrium. In addition to this standard optical lever arm, another laser (λ_2 = 810 or 845 nm) measured the tip position. The λ_2 laser was focused onto the region of the tip apex using an objective lens (numerical aperture = 1.4, 100×, oil immersion, Nikon). Backscattered light, collected by the same lens, was separated from the forward propagating light using an optical isolator [a quarter wave plate ($\lambda/4$) and a polarizing beam splitter (PBS)] and directed onto a separate QPD. Custom analog electronics output three voltages from this QPD: V_x and V_y, which are proportional to the normalized lateral differences in optical power on the detector halves, and V_z, which is proportional to the total power incident on all four quadrants. Separate line filters (not shown) placed in front of the QPDs prevented cross-talk between the lasers, which each supplied approximately 1 mW of power to the measurement point. Stabilized laser diode sources[21] were used. A small piezoelectric (pzt) actuator ($2 \times 2 \times 2$ mm^3, Physik Instrumente, not shown) affixed to the tip holder drove tapping mode oscillations. The position of the base of the cantilever and that of the sample stage were controlled by two closed-loop three-axis piezo electric stages (P363.3CD and P733.3DD, respectively, Physik Instrumente). Unless stated otherwise, experiments were performed in physiologically relevant conditions (aqueous buffer: 10 mM Tris pH = 7.6,

300 mM KCl). Two types of commercial AFM cantilevers were used (MSNL E & F, Bruker). Instrument automation was achieved using custom software (LabVIEW).

Calibration of the tip position is crucial in 3D measurements. For this purpose, a tapping tip was scanned through a 3D volume ($100 \times 100 \times 100$ nm^3) to collect the QPD detector response V_x, V_y, V_z as a function of tip position. This process took <3 min to complete. Figure 2 shows a cross section
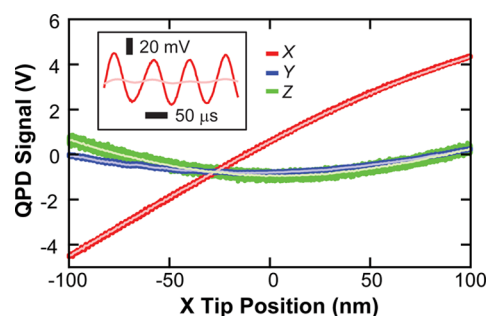

Figure 2. Tapping mode tip position calibration. Cross section of a calibration volume shows the tip position detection QPD output as a function of tip position along the x-axis (keeping y and z stationary). Dark-colored curves show full bandwidth data (V_x, red; V_y, blue; V_z, green; offset vertically for clarity). The light-colored lines are smoothed (250 Hz). Inset: detailed view of V_x in the time domain reveals several cycles of the tapping mode oscillations.

through a typical calibration volume. The tip was traveling along the x-axis and all three voltage signals are displayed. The V_x signal (red) increased approximately linearly, whereas the off-axis signals (V_y, blue; V_z, green) were relatively flat (<20% crosstalk). The 12.1 kHz tapping mode drive frequency is clearly apparent (Figure 2, inset); however, these oscillations rapidly averaged to well-defined means. For example, V_x achieved a 6 mV standard deviation in 4 ms, a noise level corresponding to 150 pm positional precision on this time scale. The averaged voltage signals (Figure 2, light lines, low pass filter corner frequency f_{lp} = 250 Hz) were used for 3D tip position calibration throughout the volume via a polynomial fitting algorithm (see Supporting Information for details). Nanoscale fiducial marks (~50 nm tall, ~700 nm diameter, amorphous silicon) patterned on the glass surface in a 10 μm grid allowed precise laser positioning along the z-axis that ensured robust and reproducible calibrations. For completeness, cross sections through the y- and z-axes of the calibration volume are also shown (Supporting Information Figure SI1).[19,22] We note that the averaged tapping mode signals are essentially identical to those acquired in contact mode, that is, in the absence of a mechanical driving force (Supporting Information Figure SI2). The root-mean-square (rms) residual error between the fits and actual position of the tip were <1 nm on each axis over the calibrated range. Thus we achieved highly linear and orthogonal detection of the tip position in the presence of tapping mode oscillations and crosstalk.

Force spectroscopy can provide a precise window into molecular-scale energy landscapes and tip trajectory mapping adds valuable new data to a traditional force spectrum. In this mode, the base of the cantilever is repeatedly advanced toward (and retracted from) a surface using a piezoelectric nano-positioning stage. In addition to recording ΔZ and its amplitude as a function of Z_{pzt} stage position (Figure 3A, gold and black, respectively), we measured the 3D position of
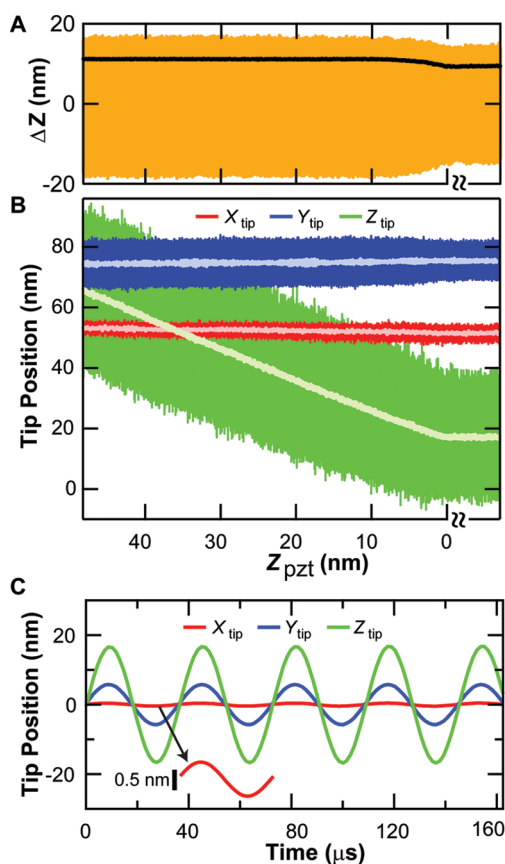
Figure 3. 3D tip trajectory during force spectroscopy. (A) The traditional observable ΔZ (gold) and its amplitude (black) plotted as a function of Z_{pzt} displacement during a tapping-mode advance curve shows the expected decrease in oscillation amplitude near the surface. The horizontal axis is discontinuous at $Z_{pzt} = 0$ nm, indicating where the tip advance was halted. (B) Simultaneously acquired 3D tip positions: X_{tip}, red; Y_{tip}, blue; and Z_{tip}, green. (C) Bandpass filtered tip trajectory plotted as a function of time when positioned 30 nm above the surface.

the tapping MSNL-F tip as it was advanced at a rate of 50 nm/s toward a clean glass surface in aqueous buffer solution (Figure 3B). As expected, the amplitude of ΔZ was reduced upon interaction with the surface. This dependence forms the basis of tapping mode imaging feedback. We note that the zero point of Z_{pzt} is arbitrary; the tip halted its advance when a

predetermined ΔZ amplitude reduction was achieved. The tip was then held in intermittent contact with the surface for a period of time and retracted and this cycle was repeated (see Supporting Information Figure SI3 for full cycle data). We note that we have also observed asymmetric behavior of the ΔZ signal during intermittent contact (Supporting Information Figure SI4), an issue which has been discussed.[23]

Simultaneously acquired 3D tip trajectory data during tip advance are shown (Figure 3B, X_{tip}, red; Y_{tip}, blue; and Z_{tip}, green). Full bandwidth data (sampling rate: 690 kHz) are drawn in dark colors; low pass filtered data ($f_{lp} = 1$ kHz) are overlaid in light. The traditional observable ΔZ yields little information when the tip is out of contact with the surface; however, Z_{tip} exhibits a steep linear slope when the tip is above the surface and advancing. The commanded tip advance rate (50 nm/s) applied to the Z_{pzt} can be compared to the locally measured rate. The disparity between them (10% in this case) becomes increasingly pronounced at low (drift-limited) pulling velocities, such as 1 nm/s or less, that have been used in state-of-the-art biophysical experiments.[24] In terms of average lateral tip positions, no significant motion was detected as the tip came into intermittent contact with the surface; however, the lateral amplitudes were altered. Interestingly, significant Y_{tip} "slipping" along the surface was measured in contact mode approach curves (Supporting Information Figure SI5), an observation which portends applications in tribology. To provide an instantaneous view of tip dynamics, we show the 3D position of the oscillating tip stationed 30 nm above the surface (Figure 3C). The data was filtered in a 1 kHz wide band about the 27.5 kHz drive frequency (i.e., high pass cut off $f_{hp} = 27$ kHz, low pass cut off $f_{lp} = 28$ kHz, fifth order). The largest amplitude observed was in the z-direction (12 nm), but the Y_{tip} amplitude was also significant (4.0 nm) owing to the angle ($\alpha = 17 \pm 1°$) built into the tip fixture of our AFM. We note that this angle ensures that the tip contacts the surface first; most commercial AFM's have built-in angles, typically ~15°. The rms amplitude of X_{tip} was 2.8 Å. Though small, this is significantly above the noise floor of the measurement, which was ~0.15 Å between 26 and 29 kHz, as determined by integrating the power spectral density (Supporting Information Figure SI6). We note that variations in conditions (e.g., drive frequency, drive amplitude, tip selection) altered the relative amplitudes of the tip trajectories.

Determining force in AFM generally requires knowledge of the cantilever spring constant. Our apparatus allowed direct
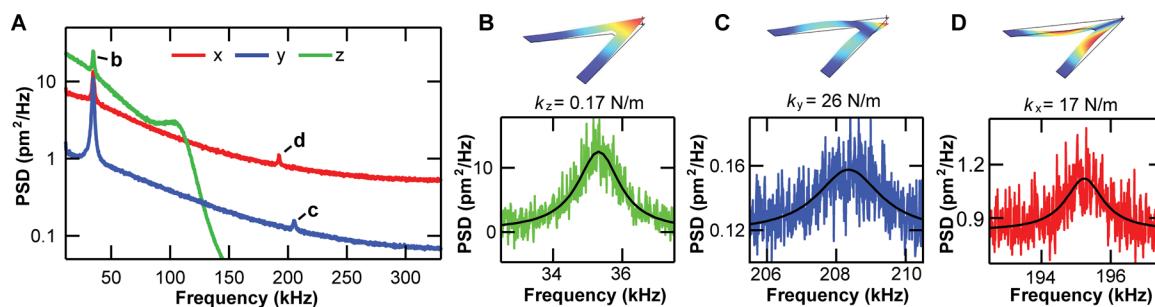

Figure 4. Measurement of cantilever spring constants in three dimensions. (A) Power spectral density of the 3D positional fluctuations of a thermally driven tip in x (red), y (blue), and z (green). Data acquired approximately 1 μm above the surface in air; the corner frequency of the z-detection electronics (100 kHz) was set lower than the two lateral channels and is clearly visible. The labeled points b, c, and d represent the resonance peaks that are magnified in panels (B), (C), and (D), respectively. The 3D spring constants and resonance frequencies were deduced from simple harmonic oscillator fits (B−D, black lines). Illustrations of the corresponding modes of the cantilever are also displayed. Note: all axes are linear, except the vertical axis of panel (A), which is logarithmic.
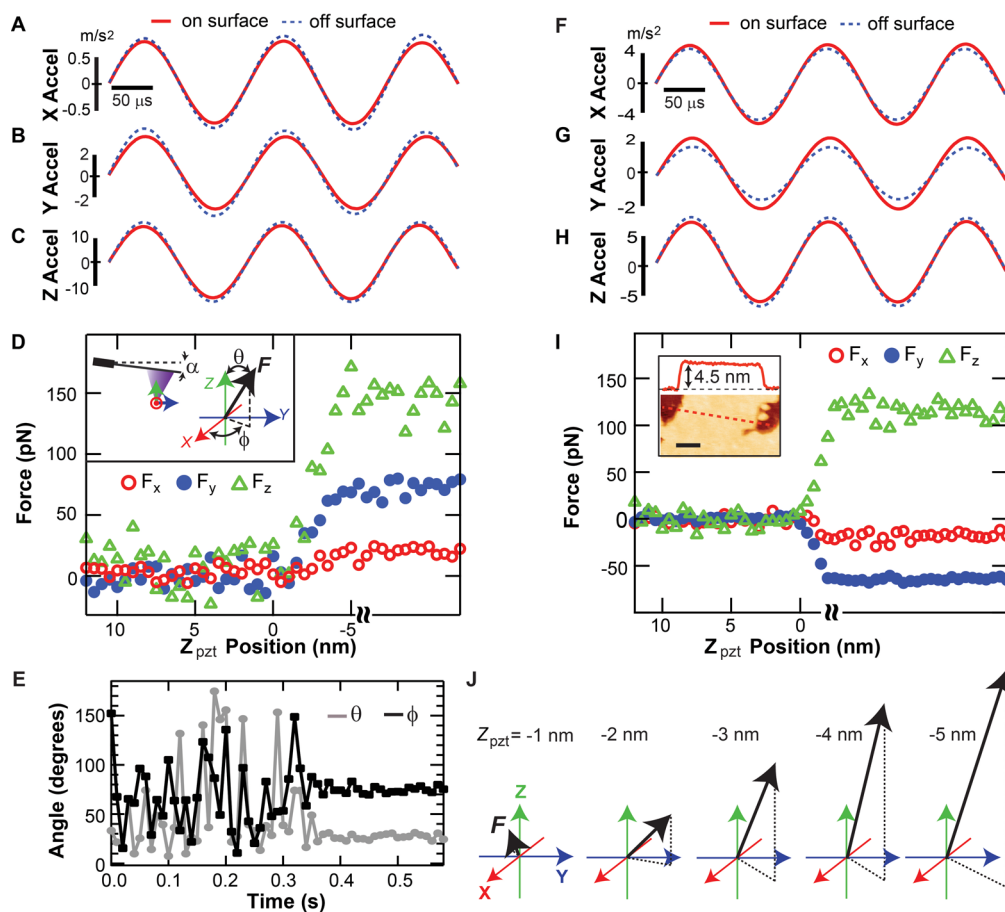
Figure 5. Interaction force vector via tip trajectory on glass and lipid. Measured 3D tip accelerations [(A) x-component, (B) y-component, and (C) z-component; bandpass filtered 1 kHz about the drive frequency: 6 kHz] are shown when in intermittent contact (red) and 15 nm above (blue dashed) a glass surface. (D) The components of the three-dimensional force as a function of the height of the tip's base, Z_{pzt}. The axis is discontinuous after $Z_{pzt} = -5$ nm, indicating where the tip advance was halted. (E) Angles θ and ϕ characterizing the 3D force vector are plotted versus time. Intermittent contact was established with the surface at $t \sim 340$ ms. The tip advance toward the surface was halted at at $t = 440$ ms. θ and ϕ are defined (D, inset) as is the static angle α built into the apparatus. (F−H) The 3D tip acceleration data acquired on and 15 nm above a lipid bilayer surface (bandpass filtered 1 kHz about the drive frequency: 9 kHz). (I) The 3D force components experienced by the tip when advanced toward the lipid membrane surface are shown. A cross section line scan (red) through an image (I, inset; scale bar = 200 nm) of the lipid sample confirms the presence of a 4.5 nm high lipid bilayer. (J) Visualizations of the interaction force vector at locations of decreasing tip−sample height above a glass surface ($Z_{pzt} = -1, -2, -3, -4$, and -5 nm, respectively) showing the rapid suppression of the force pointing noise after initial interaction with the surface.

measurement of the 3D spring constants k_x, k_y, and k_z. To achieve this, we monitored the positional fluctuations of a thermally driven tip that was stationed 1 μm above a surface at room temperature. We identified peaks in the power spectral density (PSD) of this data corresponding to three principle modes of the MSNL-E tip (Figure 4). Simple harmonic oscillator fits[25] to each of these peaks output 3D spring constants. To optimize acquisition, data was acquired sequentially on each axis, in air, and a simplified (linear) calibration procedure was used (see Supporting Information for details). The experimentally measured spring constants were k_x = 17 ± 8 N/m, k_y = 26 ± 9 N/m, and k_z = 0.17 ± 0.01 N/m (average ± σ). We used the cantilever geometry and well-known material parameters to corroborate these measurements via analytical calculations[26] as well as finite element modeling (COMSOL). In all cases, the theoretical spring constants were within a factor of 2 of experimentally determined values.

Finally, we deduced the interaction force vector directly from the measured tip trajectory $X_{tip}(t)$, $Y_{tip}(t)$, and $Z_{tip}(t)$. The second time derivative of these positions provides a straightforward means to deduce the interaction force components via Newton's second law, for example, $F_x = m_x \ddot{X}_{tip}(t)$. Figure 5A−C displays the 3D acceleration of an MSNL-E tip when positioned 15 nm above (blue dashed) and in intermittent contact with (red) a glass surface. As before, data was bandpass filtered about the drive frequency: 1 kHz window, fifth order. We take the difference between acceleration amplitudes to be proportional to the tip−sample interaction, although hydrodynamic damping from the surrounding medium could also contribute (e.g., increased viscous drag due to the fluid boundary layer).[27] An effective mass for each degree of freedom $m_x = 1.1$ (±0.5) × 10^{-10} kg, $m_y = 1.4$ (±0.5) × 10^{-10} kg, $m_z = 5.3$ (±0.3) × 10^{-11} kg, followed directly from a simple harmonic model, for example, $m_x = k_x/\omega_{ox}^2$, where ω_{ox} is the fundamental angular frequency of the x mode in fluid (Supporting Information Figure SI7). Because of the fluid, the effective mass is larger than the static mass of the beam $m_{beam} \approx 1 \times 10^{-11}$ kg, estimated from the cantilever's dimensions and density.[28]

To determine the 3D force experienced by the tip, the rms amplitude of the 3D tip acceleration was averaged for 60 ms with the tip positioned 15 nm above the surface (i.e., point of closest tip approach = 15 nm). The amplitudes of this "off surface" reference vector were 0.59 ± 0.03, 2.85 ± 0.06, and 12.1 ± 0.2 m/s^2 in x, y, and z, respectively. Subsequently, the average acceleration amplitudes (determined in continuous 10 ms time windows, ~60 tip oscillations) were subtracted from the "off surface" reference accelerations and multiplied by the appropriate effective masses to yield 3D force components as a function of Z_{pzt} position during a 50 nm/s advance curve (Figure 5D). Thus, each data point represents the average force magnitude (f_{lp} = 100 Hz) along each axis. Positive forces indicate a reduction in tip acceleration amplitudes upon interaction with the surface. When held in intermittent contact with the glass surface at Z_{pzt} = −5 nm for 0.25 s, the average magnitude of the normal force component F_z was 152 pN. This value is similar to the magnitude estimated using the traditional observable (132 pN, based on the change in ΔZ amplitude (1.10 nm) and the ΔZ measured spring constant: k = 0.12 N/m), corroborating our trajectory-based force analysis. We note that the method is limited to soft tapping applications (desirable in many biological studies) in which the DC deflection of the tip is negligible. Further, the analysis assumes that the effective masses and the viscous damping do not vary significantly over the distance (15 nm) that separates the "off surface" reference acceleration determination from the measurement point. We also note that the bandpass filtered data shown (Figure 5A−C,F−H) appear largely harmonic and symmetric. However, underlying complexity in the motion becomes evident when the filtering is relaxed (Supporting Information Figure SI8). Narrow bandpass filtering excludes higher harmonic contributions; therefore, nonlinearities are not expected to contribute to our interaction analysis.[29] In terms of precision, the rms noise for each force component was σ_x = 5 pN, σ_y = 9 pN, and σ_z = 17 pN (Δf = 4−100 Hz). This noise changed by <10% when calculated above and in intermittent contact with the surface, thus the internal feedback to the piezoelectric stages did not contribute substantially to the measured force noise.

Significant forces acted on the tip in both lateral directions. The force in the y-direction (i.e., nearly parallel to the long axis of the cantilever) achieved a maximum value of ~74 pN, which is approximately half of the value of the normal force. This is 60% larger than expected based on the angle α = 17° built into the apparatus (Figure 5D, inset). The x-component of the interaction rose to 13% of the normal force. Thus the measured force vector tilted considerably away from the surface normal.

The orientation of a vector in three-dimensional space can be defined by two angles, a polar angle $\cos \theta = (F_z/F)$ and an azimuthal angle $\cos \phi = F_x/(F \sin \theta)$, where $F = (F_x^2 + F_y^2 + F_z^2)^{1/2}$. Therefore we adopted a polar coordinate system with the origin at the tip apex (Figure 5D, inset). Figure 5E shows a time course of these two angles while the tapping tip was advanced toward the glass surface. The advance rate was held constant $\dot{Z}_{pzt}$ = 50 nm/s until t = 440 ms, at which point it was halted ($\dot{Z}_{pzt}$ = 0). As the data indicate, the direction of the interaction was ill-defined initially; however, the pointing noise of the force vector rapidly quenched at $t \sim$ 340 ms, corresponding to the onset of intermittent contact with the surface. Thus, the orientation of the force vector was established early upon interacting with the surface and was relatively stable thereafter (Figure 5 J). At Z_{pzt} = −5 nm, the

average values of the angles were θ = 28 ± 3° and ϕ = 75 ± 3°, where the uncertainty in direction (pointing noise) of the force vector is the standard deviation of the angles in a bandwidth Δf = 4−100 Hz. The static geometry built into the apparatus implied that θ should be equal to α = 17° and likewise that ϕ = 90° (the built-in angle in the x-direction equals zero). Surprisingly, our measurements revealed that θ was 11° larger than expected and ϕ differed by 15°. We note that in the current analysis, which is based on time-averaged acceleration amplitudes, an interaction emanating from the positive x-direction results in an equivalent signal to the same interaction acting from the negative x-direction. Hence, there is a 2-fold degeneracy in the assignment of angle ϕ, it is either 75 or 105° (i.e., specified up to a reflection about the y-axis).

As a final application relevant to the biophysics community, we measured the 3D tip trajectory as a tapping tip encountered a lipid bilayer surface (Figure 5F−I). Lipid vesicles consisting of 1-palmitoyl-2-oleoyl-*sn*-glycero-3-phosphocholine (POPC, Avanti Polar Lipids, Inc.) were extruded and then deposited onto clean glass surfaces (Supporting Information for details). A representative image (Figure 5I, inset) shows a ~4.5 nm step, confirming the presence of a bilayer.[30] Finally, 3D force spectroscopy was performed in a manner identical to that described for glass. While the normal force components F_z behaved similarly on the two samples, the lateral components on lipid diverged significantly from their previous behavior on glass. Interestingly, in this lipid case, the x and y acceleration amplitudes on the surface were larger than those measured 15 nm above (Figure 5F,G, compare dashed and solid lines). This gives rise to negative lateral force magnitudes in our analysis (Figure 5I, red and blue). We posit that this phenomenon is due to cantilever mode mixing facilitated by the unusual mechanical properties of the lipid bilayer, which combine high lateral mobility with significant compressibility [e.g., an effective elastic modulus $E_{lipid} \sim$ 20 MPa,[31] leads to a contact stiffness roughly 2000-fold less than glass ($E_{glass} \sim$ 50 GPa)]. We have repeated these experiments using nominally identical tips, tip holders, and lipid sample preparations. In contrast to glass surface results, which are generally consistent, the lipid experiments have yielded rich and varied behavior. In some experiments F_x goes positive upon interacting with lipid, while F_y goes negative (Supporting Information Figure SI9A); in others F_x is largely unchanged and F_y goes positive upon interacting with the lipid (Supporting Information Figure SI9B). Curiously, this diversity of tip−sample interaction behavior was observed on a relatively simple single-component lipid bilayer using nominally identical preparations (all at ~25 °C).

We studied the three-dimensional trajectory of commercial AFM tips as they interacted with glass and lipid surfaces in a widespread mode of operation: tapping mode, in aqueous solution. Upon measuring the 3D spring constants and effective masses, we determined the interaction force components as a tip came into intermittent contact with the surface. Owing to the 3D nature of the local observable, the method yielded the 3D force rapidly (10 ms, after calibration and reference acceleration determination) without the need for lateral scanning.

Direct measurement of the orthogonal force components in three dimensions provided insight into the tip−sample interaction. Though tapping mode clearly minimizes lateral forces applied to the sample compared to contact mode, our measurements indicate that these forces are still substantial,

reaching about 50% of the normal force, and lead to a tilt angle of the force vector significantly larger than the static geometry of the apparatus. The technique is currently limited to transparent surfaces as the tip position detection laser (810 or 845 nm) passes through the substrate; though shifting this wavelength further into the infrared would enable generalizing to common semiconducting substrates, for example, silicon.[32] Furthermore, the method is compatible with high speed AFM; indeed, as cantilevers become increasingly small there is growing demand for high numerical aperture optics to replace traditional optical lever arm detection schemes.[33] Direct measurement of 3D interaction forces can enhance our understanding of common AFM operations and provide a foundation for a robust 3D force probe in perturbative conditions relevant to numerous biological and chemical investigations. For example, we foresee applications in biophysics such as mapping trajectories of disordered protein structures and flexible loops,[34] which are critical facilitators of protein−protein interactions.

■ ASSOCIATED CONTENT

Ⓢ Supporting Information

A detailed description of the sample preparation and tip selection, tip position calibration, and data acquisition as well as 3D spring constant determination can be found in the Supporting Information. Further, we show tapping mode tip position calibrations in y and z, contact and tapping mode calibration comparison, full cycle force spectrum, asymmetric behavior of ΔZ during intermittent contact, lateral slipping during contact mode approach, signal-to-noise determination for X_{tip}, resonance frequency dependence on medium, detailed view of tapping tip dynamics on glass, and the diversity of 3D force components on lipid bilayers. This material is available free of charge via the Internet at http://pubs.acs.org.

■ AUTHOR INFORMATION

Corresponding Author
*E-mail: kinggm@missouri.edu.
Notes
The authors declare no competing financial interest.

■ ACKNOWLEDGMENTS

■ REFERENCES

(1) Binnig, G.; Quate, C. F.; Gerber, C. *Phys. Rev. Lett.* **1986**, *56* (9), 930−933.
(2) Bippes, C.; Muller, D. *Rep. Prog. Phys.* **2011**, *74*, 086601.
(3) Meyer, G.; Amer, N. M. *Appl. Phys. Lett.* **1988**, *53* (12), 1045−1047.
(4) Rugar, D.; Mamin, H. J.; Guethner, P. *Appl. Phys. Lett.* **1989**, *55*, 2588−2590.
(5) Meyer, G.; Amer, N. M. *Appl. Phys. Lett.* **1990**, *57*, 2089−2091.
(6) Howard-Knight, J. P.; Hobbs, J. K. *J. Appl. Phys.* **2011**, *109*, 074309.
(7) Payton, O. D.; Picco, L.; Robert, D.; Raman, A.; Homer, M. E.; Champneys, A. R.; Miles, M. J. *Nanotechnology* **2012**, *23* (20), 205704.
(8) Hoh, J. H.; Engel, A. *Langmuir* **1993**, *9*, 3310−3312.
(9) Pratt, J. R.; Shaw, G. A.; Kumanchik, L.; Burnham, N. A. *J. Appl. Phys.* **2010**, *107*, 044305.

(10) Stiernstedt, J.; Rutland, M. W.; Attard, P. *Rev. Sci. Instrum.* **2005**, *76*, 083710.
(11) Radmacher, M.; Cleveland, J. P.; Fritz, M.; Hansma, H.; Hansma, P. *Biophys. J.* **1994**, *66*, 2159−2165.
(12) Holscher, H.; Langkat, S. M.; Schwarz, A.; Wiesendanger, R. *Appl. Phys. Lett.* **2002**, *81*, 4428−4430.
(13) Ternes, M.; Lutz, C. P.; Hirjibehedin, C. F.; Giessibl, F. J.; Heinrich, A. J. *Science* **2008**, *319* (5866), 1066−9.
(14) Fukuma, T.; Ueda, Y.; Yoshioka, S.; Asakawa, H. *Phys. Rev. Lett.* **2010**, *104*, 016101.
(15) Dai, G.; Hassler-Grohne, W.; Huser, D.; Wolff, H.; Danzebrink, H.-U.; Koenders, L.; Bosse, H. *Meas. Sci. Technol.* **2011**, *22*, 094009.
(16) Abe, M.; Sugimoto, Y.; Namikawa, T.; Morita, K.; Oyabu, N.; Morita, S. *Appl. Phys. Lett.* **2007**, *90* (20), 203103.
(17) Albers, B. J.; Schwendemann, T. C.; Baykara, M. Z.; Pilet, N.; Liebmann, M.; Altman, E. I.; Schwartz, U. D. *Nat. Nanotechnol.* **2009**, *4*, 307−310.
(18) Herruzo, E. T.; Asakawa, H.; Fukuma, T.; Garcia, R. *Nanoscale* **2013**, *5* (7), 2678−85.
(19) King, G. M.; Carter, A. R.; Churnside, A. B.; Eberle, L. S.; Perkins, T. T. *Nano Lett.* **2009**, *9* (4), 1451.
(20) Hansma, P. K.; Cleveland, J. P.; Radmacher, M.; Walters, D. A.; Hillner, P. E.; Bezanilla, M.; Fritz, M.; Vie, D.; Hansma, H. G.; Prater, C. B.; Massie, J.; Fukunaga, L.; Gurley, J.; Elings, V. *Appl. Phys. Lett.* **1994**, *64* (13), 1738−1740.
(21) Carter, A. R.; King, G. M.; Ulrich, T. A.; Halsey, W.; Alchenberger, D.; Perkins, T. T. *Appl. Opt.* **2007**, *46* (3), 421−7.
(22) Churnside, A. B.; King, G. M.; Perkins, T. T. *Proc. SPIE* **2009**, *7405*, 74050H.
(23) Burnham, N. A.; Behrend, O. P.; Oulevey, F.; Gremaud, G.; Gallo, P. J.; Gourdon, D.; Dupas, E.; Kulik, A. J.; Pollock, H. M.; Briggs, G. A. D. *Nanotechnology* **1997**, *8*, 67−75.
(24) Junker, J. P.; Ziegler, F.; Rief, M. *Science* **2009**, *323* (5914), 633−7.
(25) te Riet, J.; Katan, A.; Rankl, C.; Stahl, S. W.; Buul, A. M.; Phang, I. Y.; Gomez-Casado, A.; Schon, P.; Gerritsen, J. W.; Cambi, A.; Rowan, A. E.; Vancso, G. J.; Jonkheijm, P.; Huskens, J.; Oosterkamp, T. H.; Gaub, H.; Hinterdorfer, P.; Figdor, C. G.; Speller, S. *Ultramicroscopy* **2011**, *111*, 1659.
(26) Neumeister, J. M.; Ducker, W. A. *Rev. Sci. Instrum.* **1994**, *65*, 2527.
(27) Svoboda, K.; Block, S. M. *Annu. Rev. Biophys. Biomol. Struct.* **1994**, *23*, 247−85.
(28) In the absence of damping, the ratio of the effective ("lumped") mass to the distributed mass of a cantilevered beam is 0.23; see Paul, W. J. *Mechanical Vibration*; John Wiley and Sons, Inc.: New York, 2007. On the basis of the measured (3-fold) reduction in resonance frequency in going from air to fluid, we estimate that the ratio of the effective mass in water to the distributed beam mass $m_{eff}^{H_2O}/m_{beam} = (m_{eff}^{H_2O}/m_{eff}^{air}) \times (m_{eff}^{air}/m_{beam}) \approx 10 \times 0.23 \approx 2$.
(29) Stark, R. W.; Heckl, W. M. *Rev. Sci. Instrum.* **2003**, *74*, 5111.
(30) Luckey, M., *Membrane Structural Biology*; Cambridge University Press: Cambridge, UK, 2008.
(31) Kunneke, S.; Kruger, D.; Janshoff, A. *Biophys. J.* **2004**, *86* (3), 1545−53.
(32) Appleyard, D. C.; Lang, M. J. *Lab Chip* **2007**, *7* (12), 1837−40.
(33) Antognozzi, M.; Ulcinas, A.; Picco, L.; Simpson, S. H.; Heard, P. J.; Szczelkun, M. D.; Brenner, B.; Miles, M. J. *Nanotechnology* **2008**, *19* (38), 384002.
(34) Sanganna Gari, R. R.; Frey, N. C.; Mao, C.; Randall, L. L.; King, G. M. *J. Biol. Chem.* **2013**, *288* (23), 16848−54.